Chapter 2

Model description

In this thesis, both simple parameterized models of mantle dynamical processes and more complex thermo-chemical mantle convection models are used. The models of the former type will be described in detail in chapters 4 and 5. The models of the latter type will be described below. First, the governing equations and the rheological model will be treated. This will be followed by a description of the implementation of solid state phase transitions of crustal and mantle material included in the models. Finally, the implementation of partial melting of crustal and mantle material and associated fractionation of trace elements and production of crustal material will be described.

2.1 Conservation equations

The model is described by the following transport equations derived from conservation of energy, mass and momentum, respectively, applying the extended Boussinesq approximation (Steinbach et al., 1989; De Smet et al., 1998). The first is the energy equation:

$$\rho c_p \left(\frac{\partial T}{\partial t} + u_j \partial_j T \right) - \alpha T \frac{dp}{dt} =$$

$$\tau_{ij} \partial_j u_i + \partial_j (k \partial_j T) + \rho_0 H + \frac{\Delta S}{c_p} \frac{dF}{dt} T + \sum_k \frac{\gamma_k \delta \rho_k T}{\rho_0^2 c_p} \frac{d\Gamma_k}{dt} \tag{2.1}$$

In this expression, T is the temperature, p pressure, F the degree of depletion, and H the internal heat productivity (see Table 2.1 for other symbols and section 2.5 for the definition of the degree of depletion).

Conservation of mass and momentum under the incompressibility condition implies

$$\partial_j u_j = 0 \tag{2.2}$$

From conservation of momentum and the assumption of an infinite Prandtl number we get the Stokes equation, describing viscous flow:

$$\partial_j \tau_{ij} = \partial_i \Delta p - \Delta \rho g_i \tag{2.3}$$

where $\Delta\rho$ is the density perturbation with respect to a uniform background density ρ_0 (see equation (2.8)) and Δp is the dynamic pressure perturbation with respect to a hydrostatic pressure $p_0 = \rho_0 g z$. Equations (2.1)-(2.3) are non-dimensionalized using the following expressions:

$$T = \Delta T \cdot T', x_i = h \cdot x_i', t = \frac{h^2}{\kappa} \cdot t', u_i = \frac{\kappa}{h} \cdot u_i', p = \frac{\eta_0 \kappa}{h^2} \cdot p', \tau = \frac{\eta_0 \kappa}{h^2} \tau'$$

with ΔT the temperature scale, h the depth scale, κ the thermal diffusivity, ρ_0 the density scale, g the gravitational acceleration, τ the differential stress, and η_0 the viscosity scale. A uniform thermal conductivity is assumed in the models. Potentially important effects of specifically the temperature dependence of thermal conductivity (Hofmeister, 1999), including delayed cooling of the mantle and focussing of magmatism (Schott et al., 2001; Van den Berg and Yuen, 2002; Van den Berg et al., 2003), are thus not included.

symbol	property	definition	value/unit
c_p	heat capacity at constant pressure		$1250\ \mathrm{Jkg^{-1}K^{-1}}$
Di	dissipation number	$\frac{\alpha g h}{c_p}$	
F	degree of depletion		
g	gravitational acceleration		$9.8\ \mathrm{ms^{-2}}$
H	radiogenic heat productivity		$\mathrm{Wkg^{-1}}$
h	length scale		
k	thermal conductivity	$\kappa \rho_0 c_{p0}$	$\mathrm{Wm^{-1}K^{-1}}$
R	internal heating number	$\frac{H_0 h^2}{c_p \kappa \Delta T}$	
Ra	thermal Rayleigh number	$\frac{\rho_0 \alpha \Delta T g h^3}{\kappa \eta_0}$	
Rb	compositional Rayleigh number	$\frac{\delta \rho g h^3}{\kappa \eta_0}$	
Rc	phase Rayleigh number	$\frac{\delta \rho g h^3}{\kappa \eta_0}$	
S	melt productivity function		$\mathrm{s^{-1}}$
ΔS	entropy change upon full differentiation		$300\ \mathrm{Jkg^{-1}K^{-1}}$
t	time		s
T	temperature		^{o}C
T_0	non-dimensional surface temperature		$\frac{273}{\Delta T}$
ΔT	temperature scale		^{o}C
w	vertical velocity		$\mathrm{ms^{-1}}$
z	depth		m
$z_0(T)$	temperature dependent depth of phase transition		m
α	thermal expansion coefficient		$3 \cdot 10^{-5}\ \mathrm{K^{-1}}$
Γ	phase function	$\frac{1}{2}\left(1 + \sin(\pi \frac{z - z_0(T)}{\delta z})\right)$	
δz	depth range of phase transition		m

Table 2.1: Symbols of the energy and momentum equations (2.4)-(2.6), the rheology equations (2.9)-(2.12), the depletion equation (2.7) and the fractionation equations (2.13) and (2.14).

symbol	property	definition	value/unit
κ	thermal diffusivity		$10^{-6}\ \mathrm{m^2 s^{-1}}$
ρ_0	reference density		$3416\ \mathrm{kgm^{-3}}$
$\delta\rho$	density difference upon full depletion	$\frac{\partial\rho}{\partial F}$	$-226\mathrm{kgm^{-3}}$
$\delta\rho_k$	density increase of phase transition k	$\frac{\partial\rho}{\partial\Gamma}$	$\mathrm{kgm^{-3}}$
Φ	viscous dissipation	ηe^2	$\mathrm{Jm^{-3}s^{-1}}$
B_1	diffusion creep prefactor		Pas
B_2	dislocation creep prefactor		$\mathrm{Pa^{n_2}s}$
C_0	cohesion factor		0 Pa
E_1	diffusion creep activation energy		$270 \cdot 10^3\mathrm{Jmol^{-1}}$
E_2	dislocation creep activation energy		$485 \cdot 10^3\mathrm{Jmol^{-1}}$
e_{ij}	strain rate tensor	$\partial_j u_i + \partial_i u_j$	$\mathrm{s^{-1}}$
e	second invariant of the strain rate tensor	$[\frac{1}{2}e_{ij}e_{ij}]^{\frac{1}{2}}$	$\mathrm{s^{-1}}$
$f(F)$	composition dependent viscosity prefactor		
n_1	diffusion creep stress exponent		1
n_2	dislocation creep stress exponent		3.25
n_y	yield exponent		10
R	gas constant		$8.341\mathrm{Jmol^{-1}K^{-1}}$
V_1	diffusion creep activation volume		$6 \cdot 10^{-6}\mathrm{m^3mol^{-1}}$
V_2	dislocation creep activation volume		$17.5 \cdot 10^{-6}\mathrm{m^3mol^{-1}}$
$\dot{\varepsilon}$	strainrate		$\mathrm{s^{-1}}$
$\dot{\varepsilon}_y$	yield strainrate		$10^{-15}\mathrm{s^{-1}}$
η	viscosity		Pas
η_0	reference viscosity		10^{20} Pas
η_y	yield viscosity		Pas
σ_n	normal stress		Pa
τ_{ij}	deviatoric stress tensor	ηe_{ij}	Pa
τ	second invariant of the deviatoric stress tensor	$[\frac{1}{2}\tau_{ij}\tau_{ij}]^{\frac{1}{2}}$	Pa
τ_y	yield stress		Pa
c_m^0	initial concentration of trace element m		
c_m^l	concentration of trace element m in melt		
c_m^s	concentration of trace element m in residue		
K	partition coefficient		10^{-2}

Table 2.1: Symbol definitions (continued)

This results in the following non-dimensional equations:

$$\frac{\partial T}{\partial t} + u_j\partial_j T - Di(T + T_0)w =$$

$$\partial_j \partial_j T + \frac{Di}{Ra}\Phi - \frac{\Delta S}{c_p}\frac{dF}{dt}(T+T_0) + \sum_k \gamma_k \frac{Rc_k}{Ra} Di(T+T_0)\frac{d\Gamma_k}{dt} + RH \quad (2.4)$$

$$\partial_j u_j = 0 \quad (2.5)$$

$$\partial_j \tau_{ij} - \partial_i \Delta p - (RaT - RbF - \sum_k Rc_k \Gamma_k) = 0 \quad (2.6)$$

The conservation of composition is described by

$$\frac{DF}{Dt} = S(P,T,F) \quad (2.7)$$

where D/Dt denotes the substantial derivative and S is a source function, see section 2.5.

2.2 Equation of state

Convection is driven by density perturbations of different nature. These are described by the equation of state:

$$\rho = \rho_0 \left\{ 1 - \alpha(T - T_{ref}) + \sum_k \Gamma_k \frac{\delta \rho_k}{\rho_0} + \frac{\delta \rho}{\rho_0} F \right\} = \rho_0 + \Delta\rho \quad (2.8)$$

The last three bracketed terms represent the effects of thermal expansion, phase transitions and depletion. The latter two will be discussed in sections 2.4 and 2.5.

2.3 Rheological model

The deformation of material is accounted for by three separate deformation mechanisms, which are: diffusion creep, dislocation creep, and brittle failure. The former two are described by the following equation:

$$\eta_i = f(F) B_i \exp\left[\frac{E_i + PV_i}{RT}\right] \sigma^{1-n_i} \quad (2.9)$$

which is the standard Arrhenius formulation (Karato and Wu, 1993; Van den Berg and Yuen, 1998) with the addition of a composition dependent prefactor $f(F)$. The index i indicates the flow mechanism, either 1 for diffusion creep or 2 for dislocation creep. The other symbols are explained in Table 2.1. The activation energies E_i and volume V_i are based on Karato and Wu (1993), as is the prefactor B_i, in which an assumed constant and uniform grainsize of 1 mm is incorporated. The composition dependent prefactor $f(F)$ has a value of 1 for fertile peridotite and basalt (which have the same viscosity parameters in our models). For depleted peridotite (harzburgite) we apply a prefactor value of 10 for a degree of depletion over 0.05, and a linearly increasing value between $F = 0.005$ and

$F = 0.05$ from 1 to 10. This is intended to mimic the effect of dehydration during partial melting on the viscosity (Karato, 1986; Hirth and Kohlstedt, 1996; Mei and Kohlstedt, 2000a,b).

For eclogite, the composition dependent viscosity prefactor $f(F)$ has a value of 0.1. Although Jin et al. (2001) find that for an eclogite with equal amounts of the two main constituents garnet and omphacite, the strength is comparable to harzburgite (which is hydrous in their experiments), Piepenbreier and Stöckhert (2001) find evidence in eclogite microstructures for a much lower flow strength than predicted from omphacite experimental flow laws. We translate this result to our latter viscosity prefactor value of 0.1.

The third deformation mechanism in the composite rheology model, brittle failure, is approximated by a yield mechanism which is included to approximate the effects of fracturing-like behaviour when the shear stress exceeds a certain yield stress τ_y. We use a formulation of Van Hunen et al. (2002):

$$\eta_y = \tau_y \dot{\varepsilon}_y^{-1/n_y} \dot{\varepsilon}^{(1/n_y)-1} \tag{2.10}$$

The symbols are explained in Table 2.1. We prescribe the yield stress τ_y, the yield strain rate $\dot{\varepsilon}_y$ and the yield exponent n_y. The latter describes the brittleness of the behaviour (Van Hunen et al., 2002). We apply a value of 10, which gives a reasonable approximation of pure brittle behaviour. The yield strength τ_y is determined as a function of depth using Byerlee's law (e.g. Lockner, 1995):

$$\tau_y = C_0 + \mu\sigma_n \tag{2.11}$$

in which we approximate the normal stress with the lithostatic pressure (e.g. Moresi and Solomatov, 1998):

$$\tau_y = C_0 + \mu\rho g z \tag{2.12}$$

We use a low value of 0.03 for the friction coefficient μ, consistent with results of (Moresi and Solomatov, 1998) for the mobilization of the Earth's lithosphere, and assume the cohesion term C_0 to be of minor importance and set it to 0.

The diffusion and dislocation creep viscosities are inversely added to define an effective ductile creep viscosity (Van den Berg et al., 1993) and the minimum of this value and the local yield viscosity is used for the local effective viscosity.

2.4 Solid state phase transitions

2.4.1 Basalt to eclogite phase transition

The main reason for the stability of crustal material at the surface of the Earth is its inherent reduced density compared to mantle material, which allows the crust to 'float' on top of the mantle. Under specific conditions of temperature and pressure, however, basaltic crust may undergo a series of phase transitions to develop a different mineralogy that significantly increases the density of the assemblage resulting in the high pressure

form eclogite. The transition from light to dense means a transition from buoyant to gravitationally instable, which results in a tendency of the transformed crust to sink into the mantle. In a plate tectonic setting, the dense eclogite contributes to the slab pull that is the main driving force of subduction. In a non-plate tectonic setting, it may cause delamination of the lower crust (Vlaar et al., 1994). This latter process is an important factor in several models in this thesis.

In the models, basalt is transformed into heavier eclogite upon reaching depths in excess of 30 km in our model. The kinetics of this transition are approximated assuming a constant relaxation time for the transition of 1.25 Myr. The depth of 30 km (0.9 GPa) we use is somewhat less than the depth of about 40 km (1.2 GPa) which Hacker (1996) states as the minimum pressure of basalt to eclogite transformation. However, as we are dealing with melt products in a mantle that is hotter than the present, their composition is more MgO-rich (more towards komatiitic composition) than present day mid ocean ridge basalt (Nisbet, 1982). Experiments of Green and Ringwood (1967) have shown that the transition may occur at lower pressures and higher temperatures in MgO-rich rocks. Furthermore, lower pressure phase assemblages (above 0.7-0.8 GPa) may also contain garnet (Green and Ringwood, 1967; Ito and Kennedy, 1971; Hacker, 1996), thus raising the bulk density above that of the original basaltic phase assemblage. Phase boundary topography due to temperature effects is not taken into account, since this is expected to be dominated by kinetic effects because of the relatively low Clapeyron slope of about 1 MPa/K (Philpotts, 1990).

2.4.2 Mantle phase transitions

The phase transitions around 400 and 670 km depth are also taken into account separately for peridotite and eclogite, though without kinetics, assuming an equilibrium condition, which is a good approximation, particularly in a hotter Earth (Schmeling et al., 1999). The relevant parameters for these phase transitions are specified in Table 2.2. The phase transition is assumed to take place over a depth range, specified in Table 2.2. The phase function Γ_k for phase transition k is parameterized as a harmonic function over this depth range between 0 and 1, see Table 2.1. The latent heat consumption associated with the phase transitions is taken into account in the last term of equation (2.1), following Christensen and Yuen (1985). The phase transition of eclogite into perovskitite lithology in the shallow lower mantle (e.g. Ringwood and Irifune, 1988; Irifune and Ringwood, 1993; Hirose et al., 1999) is not taken into account.

Dynamic effects have been predicted of the density inversion between eclogite and postspinel peridotite in the uppermost lower mantle (Irifune and Ringwood, 1993) caused by the deeper position of the phase transition of eclogite relative to the postspinel transition of peridotite. As recent work has indicated that the transition takes place around 720 km depth (Hirose et al., 1999) rather than around 800 km (e.g. Irifune and Ringwood, 1993), and has a positive Clapeyron slope which would lift the phase transition to even shallower levels in a cool sinking eclogite body, Hirose et al. (1999) predict that a body of basaltic crust with perovskitite lithology would remain negatively buoyant and sink into the deeper mantle'. Earlier numerical experiments of Christensen (1988) show that an

transition	material	P_0 (GPa)	T_0 (K)	γ (Pa/K)	δz (km)	$\frac{\delta\rho}{\rho_0}$
400	peridotite	13.4	1756	$3 \cdot 10^6$	50	0.05
400	basalt	12.5	1747	$3 \cdot 10^6$	150	0.10
670	peridotite	22.4	1854	$-2.5 \cdot 10^6$	50	0.05

Table 2.2: Parameters of the phase transitions used in the models, based on Ringwood and Irifune (1988) and Irifune and Ringwood (1993). The first column indicates the approximate depth of the transition. P_0 and T_0 are the reference temperature and pressure for the phase transition, defining it in combination with the constant Clapeyron slope γ. The column marked δz indicates the depth range over which the transition is smeared out in the model and the last column gives the relative density contrast of the phase transition.

eclogite layer trapped in this density inversion zone in the uppermost lower mantle would probably not survive in a convecting mantle. Recent experiments by Kubo et al. (2002), however, indicate that slow kinetics of the lower mantle phase transition of basaltic material may delay the transition on the order of 10 million years, which may increase the residence time and depth extent of the shallow lower mantle density inversion zone. The density effects of the varying phase transitions are accounted for in a phase contribution term in the equation of state (2.8), scaled by the phase Rayleigh number Rc, in the momentum equation (2.6).

2.5 Partial melting of peridotite and basalt

Because of the presence of different phases in mantle peridotite, it does not have a single melting temperature, but melting takes place over a range of temperatures for a fixed pressure (see Figure 2.1). As a consequence, melting in the mantle is generally only partial because temperatures sufficient for complete melting are not reached. Another consequence is that the composition of the residual rock is a function of the degree of partial melting. The resulting melts for low degrees of partial melting are of basaltic composition (Jaques and Green, 1980; Herzberg and Zhang, 1996), changing to komatiitic compositions for higher degrees of melting (Walter, 1998).

Partial melting is modelled as an (irreversible) increase in the *degree of depletion F*, which is defined here as the mass fraction of melt produced from an initially unmelted material control volume of mantle peridotite. The extraction of melt from the source rock is described by two-phase flow models, for which different mathematical descriptions have been developed and applied in numerical models (McKenzie, 1984; Spiegelman, 1993a,b; Ogawa, 1997; Bercovici et al., 2001; Ricard et al., 2001). In this work, this is approximated by assuming all melt to be instantaneously segregated to the surface, similar to the approach of Ogawa (1988), see section 2.7. Compaction of the matrix due to the removal of melt is not taken into account. This results in an overestimate of the volume of depleted residual material (De Smet, 1999).

Evolution of the degree of depletion is described by equation (2.7). The source function S in (2.7) describes the distribution of the rate of partial melting. It applies a simple parameterization of the melting phase diagram of mantle peridotite (De Smet et al., 1998) in computing the local equilibrium degree of depletion and irreversibly updating actual local degree of depletion values accordingly. The corresponding latent heat effect results in extra terms in the energy equation, see appendix B. We use third order polynomial parameterizations of the solidus and the liquidus of mantle peridotite, based on Herzberg and Zhang (1996), down to a depth of 400 km (see Figure 2.1), assuming that melt produced below this depth is not segregated. Our isobaric melting curve, which is based on data presented by Jaques and Green (1980), is linear (see De Smet et al., 1998).

Many of the felsic rocks found in the Archean are plutonic or metamorphosed rocks that belong to the Tonalite-Trondhjemite-Granodiorite or TTG suite (Goodwin, 1991). These are thought to be formed by partial melting of metabasalts (Rapp et al., 1991). On the basis of trace element partitioning, Foley et al. (2002) and Foley et al. (2003) found that most TTG's have been formed by partial melting of metabasalts or metagabbros in the amphibolite facies, leaving behind an eclogitic residue.

Therefore, the partial melting of material of a basaltic composition, formed in the model by partial melting of mantle peridotite, is also included. A simplified phase diagram similar to that of peridotite in our model is used, assuming the melt residue is increasingly depleted in 'felsic material' which makes up the melt. We use a fifth order polynomial parameterization of the solidus and liquidus of Green (1982) for hydrated tholeiite (5 wt.% water), see Figure 2.1.

The density of mantle material is related to the degree of depletion F (Jordan, 1979). In the buoyancy term of the Stokes equation (2.6), we use a linearized parameterization of the composition dependent density (Vlaar and Van den Berg, 1991), and the coefficient $\partial\rho/\partial F$ enters the compositional Rayleigh number Rb, in the momentum equation (2.6) (see also De Smet et al., 1998, 2000b). We assume all melt to be removed instantaneously to shallower or surface levels. Because of this assumption, we neglect the buoyancy effect of melt retention, which leads to an underestimate of the buoyancy term (e.g. Scott and Stevenson, 1989; Buck and Su, 1989; Jha et al., 1994). This partly cancels the overestimation of the volume of depleted residue mentioned above.

2.6 Fractionation of trace elements

The behaviour of a single incompatible trace element is monitored in the models using Lagrangian particle tracers. Upon partial melting, the concentration of the trace element is adjusted in each tracer using an equilibrium melting formulation (see e.g. Philpotts, 1990) for each integration time step (which implies that we assume equilibration between the melt and the residue during an integration time step, and consider a new batch of melt in the following time step):

$$c_m^l = \frac{c_m^o}{F + K_m(1 - F)} \tag{2.13}$$

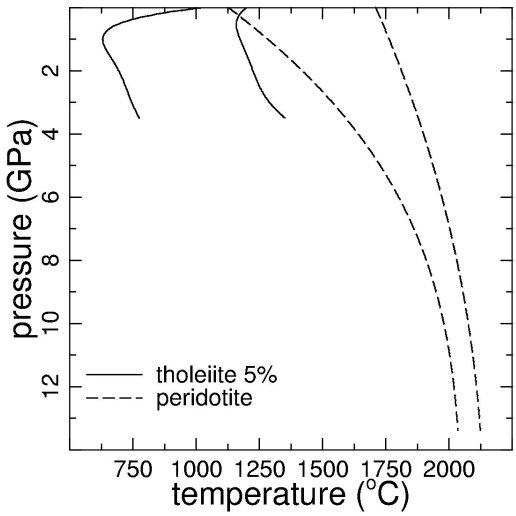

Figure 2.1: Solidus and liquidus for peridotite and basalt (tholeiite, assumed to be hydrated) used in the model calculations. The peridotite curves are based on Herzberg and Zhang (1996), the basalt curves on Green (1982), representing a tholeiite with 5 wt.% water.

$$c_m^s = K_m c_m^l \tag{2.14}$$

with c_m^s and c_m^l the mass concentrations of trace element m in solid (residue) and liquid (melt), c_m^o the initial concentration before fractionation, F the melt fraction and K_m the distribution coefficient.

The result of the above is that an enriched crust (generally by a factor 5-20) and a depleted residual mantle are formed. The internal heating rate is a function of the trace element concentration in the models. The most important heat producing species in the Archean mantle are U, Th and K. The former two have bulk partition coefficients of $1.1 \cdot 10^{-4}$ and $1.7 \cdot 10^{-4}$, respectively, for spinel peridotites in equilibrium with a basaltic melt (Beattie, 1993), though temperature, composition, oxygen fugacity and the presence of volatiles may influence these values. The partition coefficients for K between olivine and basalt, orthopyroxene and basalt and clinopyroxene and basalt are 0.007, 0.01-0.02 and 0.03, respectively (Henderson, 1982). We prescribe a distribution coefficient of 10^{-2} for the single incompatible heat producing element in our model which represents U, Th and K. This value of the partition coefficient is consistent with values for K, but somewhat larger than the values mentioned above for spinel peridotites for U and Th. It is however small enough to allow significant fractionation and thus redistribution of heat productivity, but not so small that different degrees of melting result in the same residue concentrations of virtually zero. This allows the evaluation of the development of our trace element in a

more general sense rather than limited to U, Th and K.

2.7 Crustal growth

The melt that is produced is extracted instantaneously and deposited at the top boundary, where the melt flux is transformed into an inflow boundary condition, thus producing a basaltic crust in the case of melting of peridotite, and a felsic crust in the case of melting of basalt or eclogite. This approximate melt segregation scheme is represented in Figure 2.2.

Isotope mass concentrations for the two types of melt are calculated separately in the melting column and resulting averaged (weighed using the melt mass fractions) concentrations are assigned to the respective inflowing crustal materials.

In the current approximation, the compaction of the residual mantle due to the melt removal is neglected. An estimate of the magnitude of the error in the energy balance which is thus introduced is calculated in Appendix A.

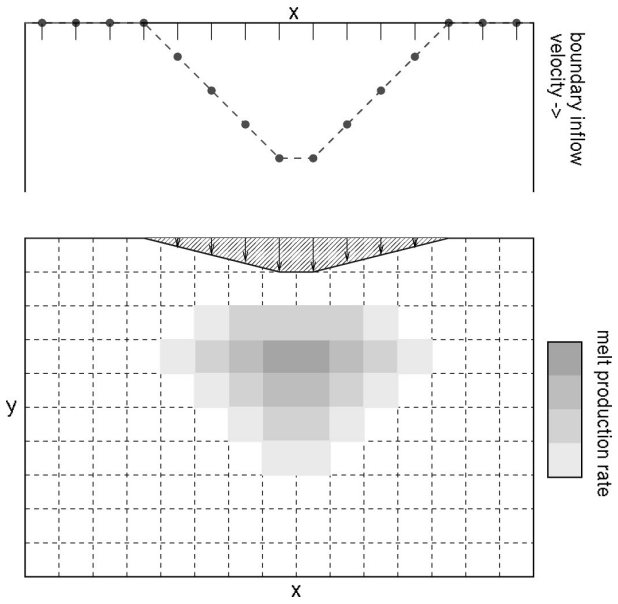

Figure 2.2: Graphical representation of the approximate melt segregation scheme employed in the numerical models. The degree of partial melting, indicated in grey tones, is integrated column-wise and transformed into an inflow velocity for the top boundary. Basaltic and/or felsic material enters the computational domain here, depending on the (relative amounts of) material that is melting below the regions of inflow.